Atomic Scale Oxidation of Silicon Nanoclusters on Silicon Carbide Surfaces

W. Chen,[†] X. N. Xie,[‡] H. Xu,[‡] A. T. S. Wee,[‡] and Kian Ping Loh*[,†]

Department of Chemistry, National University of Singapore, 3 Science Drive 3, Singapore, and Department of Physics, National University of Singapore, 2 Science Drive 3, Singapore

Received: April 16, 2003; In Final Form: August 15, 2003

The initial stage adsorption of molecular oxygen on the 6H−SiC(0001)-3×3 surface has been studied using scanning tunneling microscopy (STM) and X-ray photoelectron spectroscopy. STM filled-state imaging reveals the sequential appearances of dark sites upon initial oxygen exposure at room temperature, followed by the appearances of bright sites at higher oxygen exposures. The changes in the STM images are interpreted on the basis of changes in the local density-of-states of the silicon adatom cluster site following the sequential development of different oxygen chemisorption states, beginning with the attachment of oxygen on the dangling bond site to its subsequent insertion in the Si−Si back-bond. Periodic density functional theory calculations supported our interpretations because the most stable chemisorption site was found to occur on the reactive adatom cluster site, as opposed to the adlayer coplanar bonds. The interaction of atomic O beam with the 3 × 3 surface results in the formation of silicon oxide nanoclusters.

1. Introduction

Silicon carbide (SiC) is a promising wide band gap semiconductor for applications in high-power and high-temperature electronic devices. Besides its highly desirable properties, SiC is the only compound semiconductor that can be thermally oxidized to form SiO_2. However SiC exhibits worse electrical passivation characteristics compared to Si due to the presence of silicon oxycarbide species that produce interface states at the oxide/SiC interface. For this reason, studies of the oxidation mechanism and chemical composition of thermally grown oxides on SiC have attracted a lot of attention recently.[1−4] Fewer studies have been directed toward the low-temperature adsorption of oxygen on reconstructed, silicon-rich 6H−SiC-3×3 even though this is fundamentally interesting from the viewpoint of forming periodic silicon oxide nanoclusters. The 6H−SiC-3×3 reconstruction is an interesting superstructure that has attracted intense fundamental interests recently due to its structural complexity. Several models, including the dimer-adatom-stacking fault (DAS) model,[5] modified DAS model,[6] and twisted Si−adlayer model[7,8] have been proposed to explain its atomic structure. Technologically the 6H−SiC-3×3 structure is important as a template for the epitaxial growth of GaN and SiC,[9,10] and exhibits electronic properties such as the Mott Hubbard states.[11]

The complexity of the 6H−SiC-3×3 structure[7,8] offers several possible chemisorption sites for O_2 which are distinct from the well-studied Si(111)-7×7. Possible sites for chemisorption include (i) dangling bond site of the tetracluster, (ii) insertion into Si−Si bonds between the second and third Si adlayers, and (iii) coplanar bond sites in the third Si adlayer. So far, there are few studies on the energetic and structure of these sites. The closest experimental insight comes from the scanning tunneling work of Amy et al.,[12] who interpreted the changes in their images as due to the chemisorption of O_2 on the adlayer coplanar bonds, instead of the topmost dangling bonds. In this work, we report our results on the systematic study of the energetics, equilibrium geometry and possible reaction pathways of O_2 chemisorption on the SiC-3×3 structure using periodic density functional theory, in situ scanning tunneling microscopy (STM) and X-ray photoelectron spectroscopy (XPS). The effect of atomic O generated from an atom beam source on the surface structure of 6H−SiC was also investigated using STM and XPS.

2. Experiment

The 6H−SiC(0001) oxidation experiments were conducted in a UHV chamber with a base pressure of 2×10^{-10}mbar, which allows in situ transfer between facilities for scanning tunneling microscopy (STM), X-ray photoelectron spectroscopy (XPS), and low energy electron diffraction (LEED). The 6H−SiC (0001) sample (CREE Research Inc) was prepared by annealing it at 850 °C under a Si flux for 2.5 min, resulting in a 3 × 3 SiC surface reconstruction as determined by STM and LEED, details of which have been previously reported.[13,14] Molecular O_2 was dosed on the 3 × 3 SiC surface by backfilling the chamber to a pressure that did not exceed 2×10^{-9} mbar, using a precision leak valve. The dosage was quoted in langmuirs, where 1 langmuir = 1.33×10^{-6} mbar·s. The substrate temperature was maintained at room temperature during dosing. In addition to molecular oxygen dosing, we also carried out atomic oxygen beam treatment of the surface. For this, the 3 × 3 SiC surface was exposed to atomic oxygen generated from a remote-discharged radio frequency plasma atom beam source,[15] in a flow pressure of 5.0×10^{-5} mbar for 20 min. All thermal processing in our UHV chamber was performed using direct resistive heating and the temperature was measured by an optical pyrometer. Calibration of the scanner in the STM was performed using atomically resolved images of the well-known Si (111)-7 × 7 surface.

The 6H−SiC(0001)-3×3 reconstruction was modeled using a periodic slab with a 3 × 3 surface unit cell. The periodic DFT calculation was performed using the CASTEP code where a plane-wave basis set and conjugated gradient electronic minimization were used.[16] Geometrical optimization was carried out using the Broyden−Fletcher−Goldfarb−Shanno (BFGS) routine.[17] The exchange and correlation energies were calculated with the Perdew−Wang form of generalized-gradient approximation (GGA).[18] Vanderbilt's ultrasoft pseudopotentials were used. Special *k*-points were generated with *k* spacing of 0.05 Å^{-1} using the Monkhorst−Pack scheme. The accuracy of the method was tested by performing the single point energy

* To whom correspondence should be addressed: Prof. Kian Ping Loh, email: chmlohkp@nus.edu.sg; FAX: (65) 67791691.
[†] Department of Chemistry, National University of Singapore.
[‡] Department of Physics, National University of Singapore.

10.1021/jp035029e CCC: $25.00
Published on Web 09/25/2003

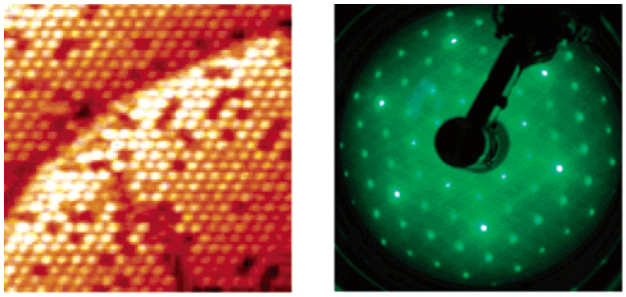

Figure 1. (a) STM filled state topography for the 6H−SiC(0001)-3×3 surface (200Å × 200 Å). (I = 0.30 nA; V_T = 2.2 V). (b) LEED pattern of this clean surface. (Electron beam energy = 100 eV.)

calculation whereby optimized bulk cell parameters were compared with the experimental ones to achieve a discrepancy of less than 1%. In the geometrical optimization, the topmost bulk Si−C bilayer and Si adatoms were allowed to relax, while the other five Si−C bilayers were maintained at their bulk positions. The plane−wave cutoff energy was set to 310.0 eV in the converged calculations.

3. Results and Discussion

3.1. STM and XPS Results. Figure 1a shows a 600 Å × 600 Å STM filled state image of the clean 6H−SiC(0001)-3×3 surface. Spherical protrusion which adopts a hexagonal array with a 3 × 3 periodicity can be seen. These protrusions have been interpreted to represent the adatom + trimer structure in each unit cell.[7,8] The terraces on the SiC surface are fully covered by these 3 × 3 unit cells although some vacancy defects are observable. The corresponding LEED image of the 3 × 3 surface is shown in Figure 1b. Small spot XPS was employed to follow the oxidation process throughout to monitor the gradual uptake of the oxygen on the initially oxygen-free surface.

During the initial oxidation experiment, all STM images were acquired with a positive tip bias (filled state) and a low tunneling current (0.1 nA). Although the images observed under this condition were not as clear as those observed at a high tunneling current (0.3 nA) as shown in Figure 1, the oxygen decomposition process induced by energetic tunneling electrons is minimized. The STM filled state images of the same area for the 6H−SiC-(0001)-3×3 surface that was exposed to oxygen at 0.2, 1, and 2 langmuirs at room temperature are also shown in Figure 2, parts b−d, respectively. During the initial stage of oxidation at room temperature, the 3 × 3 structure was seen to maintain its structure. The consequence of a low dose of oxygen was to result in the appearance of dark sites initially, as shown in Figure 2b. This may be similar to the "D" site that has been reported by Kubo et al.[28] in their study of the room-temperature oxidation of 6H−SiC(0001)-3×3. With increasing oxygen dose, the population of the dark sites increased, and at the same time, bright sites appeared as well, as indicated in Figure 2c. These bright sites have not been previously reported. The bright sites were observed to form around the vicinity of the preexisting dark sites. The population of the dark sites remained stable after exposure to 2 langmuirs of O_2 (Figure 2d), while the population of the bright sites continued to increase. At higher O_2 exposure (>10 langmuirs), the reconstruction was lifted. The 3 × 3 reconstruction could be recovered following a subsequent anneal to 850 °C. On the recovered 3 × 3 surface, cluster-like bright spots could be observed in the STM filled state image, and we attribute these to silicon oxide clusters (Figure 2e) formed by the diffusion of segregated silicon and oxygen species at high temperature.

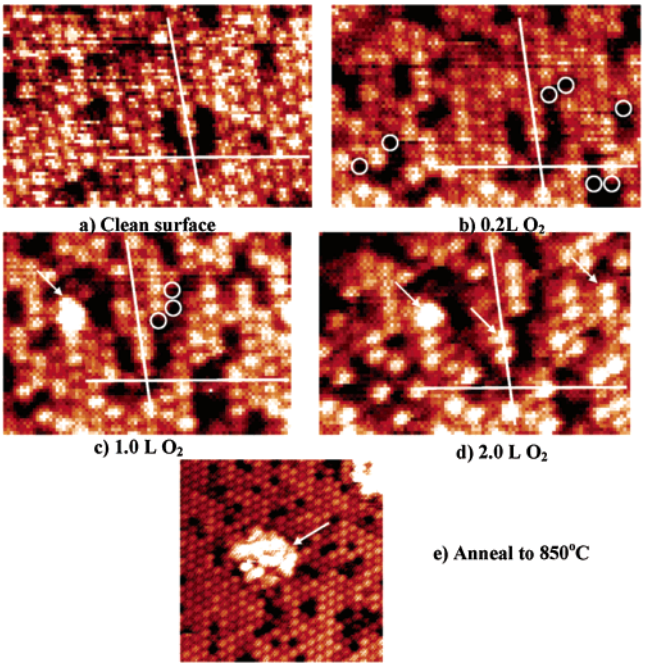

Figure 2. (a) 150 Å × 100 Å STM filled state topography of the 6H−SiC(0001)-3×3 clean surface and oxygen-exposed at (b) 0.2, (c) 1, and (d) 2 langmuirs (150 Å × 100 Å) Note the appearance of more dark spots (highlighted by circles) with increasing O_2 dose. Note the subsequent appearance of white spots, highlighted by arrows. (e) Aggregation of the white spots into a cluster after annealing to 850 °C (200Å × 200 Å). I = 0.10 nA; V_T = 2.2 V.

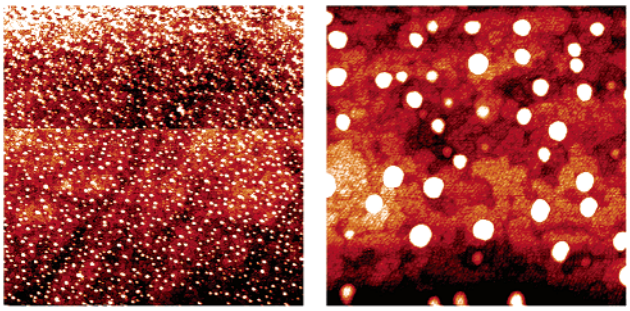

Figure 3. 2000 nm × 2000 nm (left) and 400 nm × 400 nm (right) STM filled state topography for the 6H−SiC(0001)-3×3 surface after atomic O treatment at room temperature for 20 min, and subsequently annealed to 1300 K, resulting in the formation of SiO nanoclusters (30−50 nm).

The effect of atomic O on the surface was also investigated by STM. Figure 3 displays STM filled state images for the 6H−SiC(0001)-3×3 surfaces after atomic O-treatment at room temperature. Atomic O has an etching effect on the surface, resulting in a rough surface initially, but regular-sized nanoclusters were formed after subsequent annealing to elevated temperatures. These clusters were monodispersed on the SiC surface with sizes of about 30−50 nm and remained stable even by annealing to 1000 °C. On the basis of the results of TOF−SIMS analysis, the chemical composition of these nanoclusters is identified to be silicon oxide (SiO_2). The root-mean-square roughnesses of the surface at different stages of the oxygen treatment have been evaluated by scanning tunneling microscopy and the results tabulated in Table 1.

In situ XPS was also performed to verify the chemical binding state of the oxygenated states arising from both molecular and atomic oxidation. Figure 4 shows a chemically shifted component located at 101.9 eV in the Si 2p core level peak, formed after 4 langmuirs of O_2 was dosed on the surface. The bulk

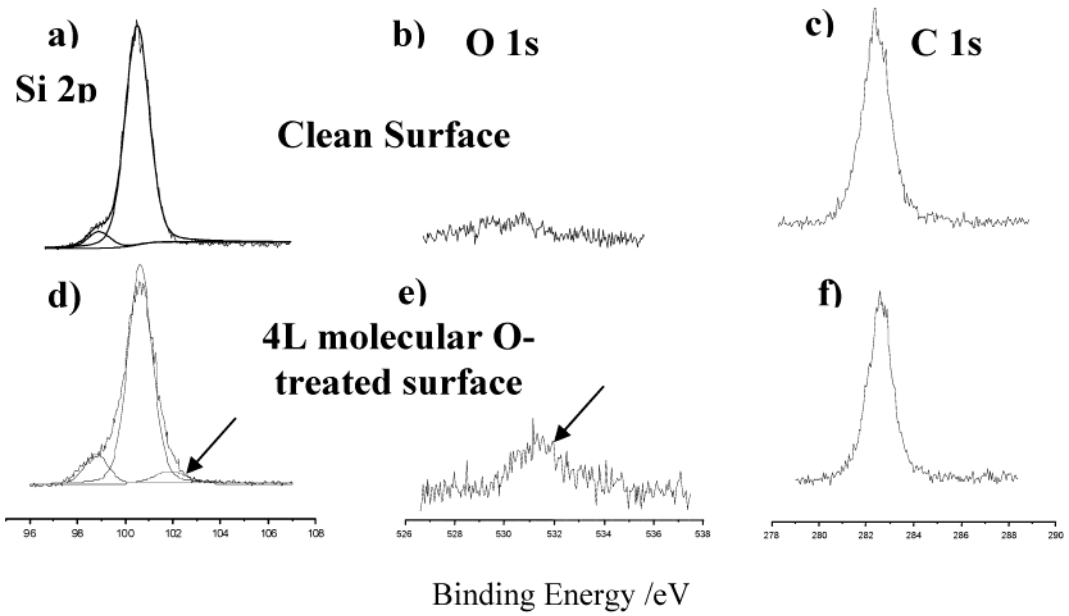

Figure 4. Si 2p, O 1s, and C 1s core level XPS peak for 6H−SiC(0001)-3×3 clean surface (a, b, and c) and 4-langmuir molecular O-treated surface (d, e, and f).

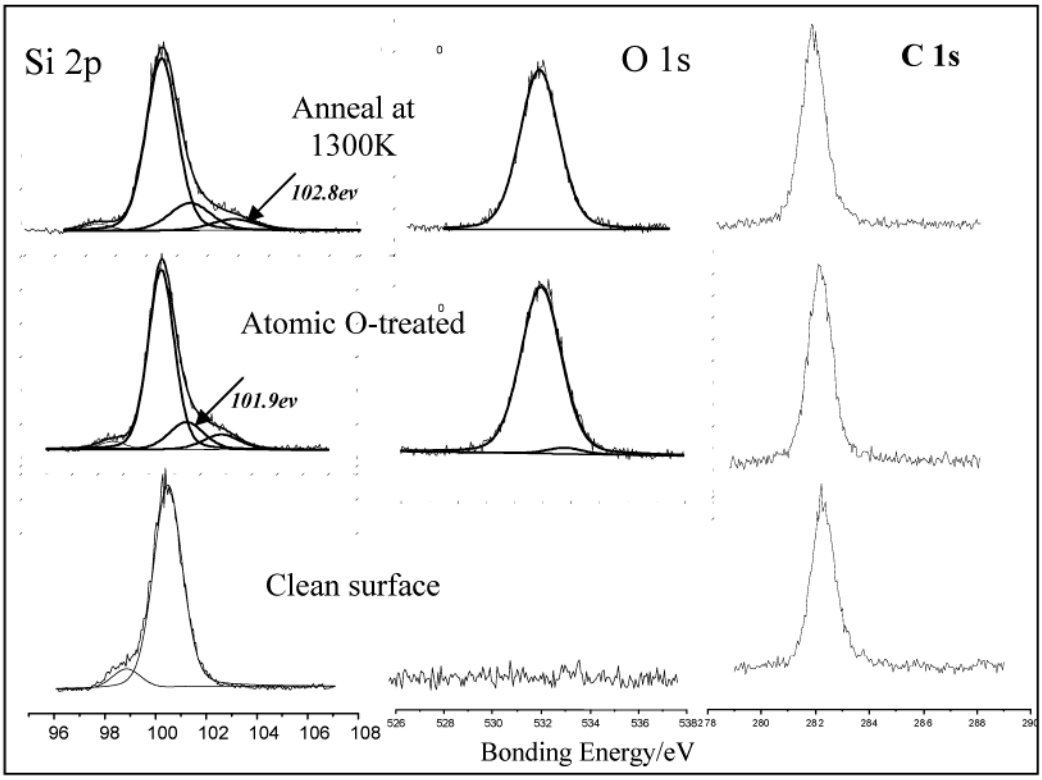

Figure 5. Si 2p, O 1s, and C 1s core level XPS peak for atomic O-treated 6H−SiC(0001)-3×3 surface.

TABLE 1. Root-Mean-Square Roughness of the Surface Evaluated by Scanning Tunneling Microscopy

	clean surface	molecular O_2 adsorption	after annealing the O_2-dosed SiC sample	atomic O-treated sample
RMS (Å)	0.81	1.20	0.83	14.50

peak at 100.2 eV and a surface shifted component at 98.6 eV is associated with the Si adatom + trimer structure of the 3 × 3 model.[12,19,20] The new component at 101.9 eV was assigned to a partially oxidized state of Si (Si^+, Si^{2+}) because a fully oxidized Si^{4+} state (SiO_2) component is expected to have a chemical shift 2.7 eV higher than the bulk Si 2p peak of SiC,[20] but this was not observed. For the C 1s peak (Figure 4c,f), no apparent chemical shift was observed after oxidation suggesting that carbon did not participate in room-temperature initial molecular oxidation process.

Figure 5 shows the changes in the Si 2p, O 1s, and C 1s core levels following treatment by atomic oxygen. Two new chemically shifted components located at 101.9 and 102.8 eV can be seen in the Si 2p spectrum in Figure 5. The peak at 101.9 eV

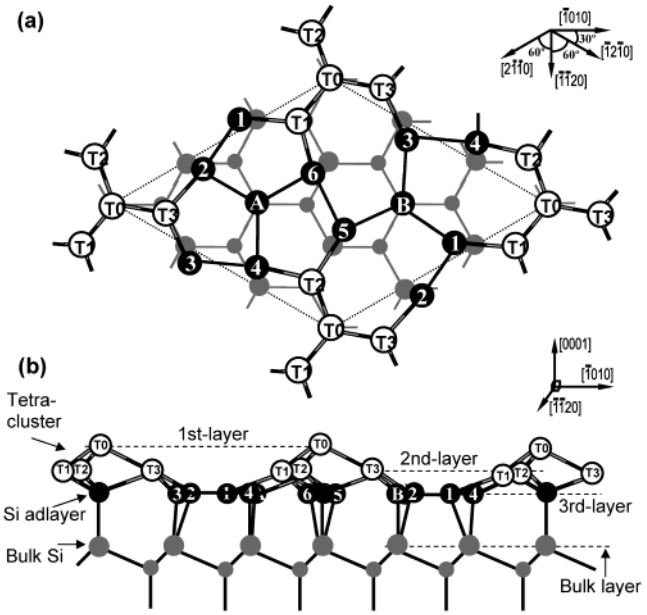

Figure 6. Top (a) and side (b) views (in [$\bar{1}\bar{1}$20] azimuth) of twisted Si adlayer model for 6H−SiC(0001)-3×3 surface according to the Starke model.[7,8]

can be assigned to Si^{+} or Si^{2+}, while the peak at 102.8 eV can be assigned to Si^{4+}.[19,22,23] In Figure 5, no major chemical shift of C 1s is observed after oxidation, suggesting that only silicon oxide species, and not silicon oxycarbide species, are formed. The Si^{4+} states were found to be very stable because this peak intensity did not decrease much even after annealing to 1000 °C (Figure 5a).

3.2. Periodic DFT Calculations. A periodic DFT calculation using the CASTEP code was carried out to investigate the thermodynamically favored oxidation products on the 6H−SiC-(0001)-3×3 surface. There are two possibilities here that we wish to distinguish with regard to the first site of attachment by oxygen. Will oxygen attach to the silicon adatom site first, or will it attach to the coplanar adlayer site below? Figure 6 shows the 6H−SiC(0001)-3×3 twisted reconstructed model, proposed by U. Starke et al.[7,8] The top layer comprises the Si adatom + trimer structure; the second layer is the twisted Si adlayer above the bulk SiC substrate. The surface basically consists of three Si adlayers. The tetracluster containing T0, T1, T2, and T3 atoms constitute the first and second adlayer. There is one dangling bond located on the first adlayer as shown. In the third layer, atom A is located in the center of the 9-membered ring while atom B is located in the center of a 15-membered ring. The optimized geometry reproduced the essential features of the twisted Si adlayer structure.[7,8] Essentially, the tetracluster is rotated by 9°, the bonding angles of the topmost T0 atom to the three supporting T1, T2, and T3 atoms is around 86−87°, deviating considerably from the typical tetrahedral bonding of 109.5°.

In the calculation of O_2 adsorption on the SiC 3 × 3 surface, we systematically examined the geometry and energetic for successive O_2 uptake onto all possible chemisorption sites of the 3 × 3 unit cell. In the initial oxygenation stage, the various possibilities for the binding of the oxygen on the adatom cluster are shown in Figure 7. Models C1 and C2 both designate the "on-top" oxygen mode where the dangling bond is consumed by molecular O_2. If the O−O bond is broken, and insertion of O into the back-bonds of the tetracluster occurs, two models such as C3 and C4 are considered. Model C7 is the resulting structure following the chemisorption of two oxygen molecules.

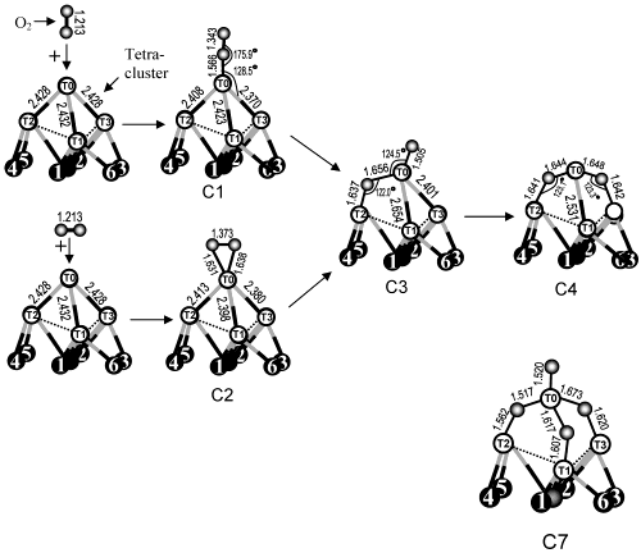

Figure 7. Possible configurations (viewed in [2$\bar{1}\bar{1}$0] direction) and pathways of one O_2 per 3 × 3 unit cell at the tetra-cluster dangling bond site of the SiC(0001)-3×3 surface. Model C7 has four oxygen atoms attached to T0 and is due to the chemisorption of two oxygen molecules.

TABLE 2. Calculated Chemisorption Energy for SiC-3×3 + xO_2 = SiC-3×3:2xO Reactions

oxygen coverage, C (ML)	surface models	chemisorption energy, ΔE (eV/unit cell)
$x = 1$, $C = 2/9$	C1	−4.10
3×3:2O surface	C2	−4.32
	C3	−5.61
	C4	−6.93
	A1	−3.52
	A2	−3.48
	A3	−3.50
	A4	−3.51
$x = 2$, $C = 4/9$	C5	−10.33
3×3:4O surface	C6	−10.45
	C7	−11.53
	A5	−9.07
	A6	−9.14
$x = 3$, $C = 6/9$	A7	−13.49
3×3:6O surface	A8	−14.07
	A9	−14.56
	A10	−14.72

Possible configurations for O_2 adsorption onto atom A and B on the adlayer site are shown in Figure 8. In Figure 8, the adlayer structures include the following: A1 model with O-insertion into A-2 and 1−2 bonds; A2 model with O-insertion into A-2 and A-6 bonds; A3 model with O-insertion into B-3 and 3−4 bonds; and A4 model with O insertion into B-1 and B-3 bonds. Following geometry optimization, we found that the bridging oxygen structure Si−O−Si is always formed.

The calculated chemisorption energy for SiC-3×3 + O_2 → SiC-3×3:2O based on different structural models are tabulated in Table 2. Two important results emerge from the calculations: (1) The heats of reaction to yield structure C4 and C3 are found to be the highest, and (2) chemisorption energies for the adsorption of oxygen on the adatom cluster site involving atoms T0, T1, T2, and T3 are higher than that of atoms A and B in the adlayer site. Among the different SiC-3×3:2O structural models, the C4 model is more exothermic by ∼3.4 eV/unit compared to the adlayer models. This clearly indicates that the initial oxygen adsorption on the cluster site is energetically more favorable.

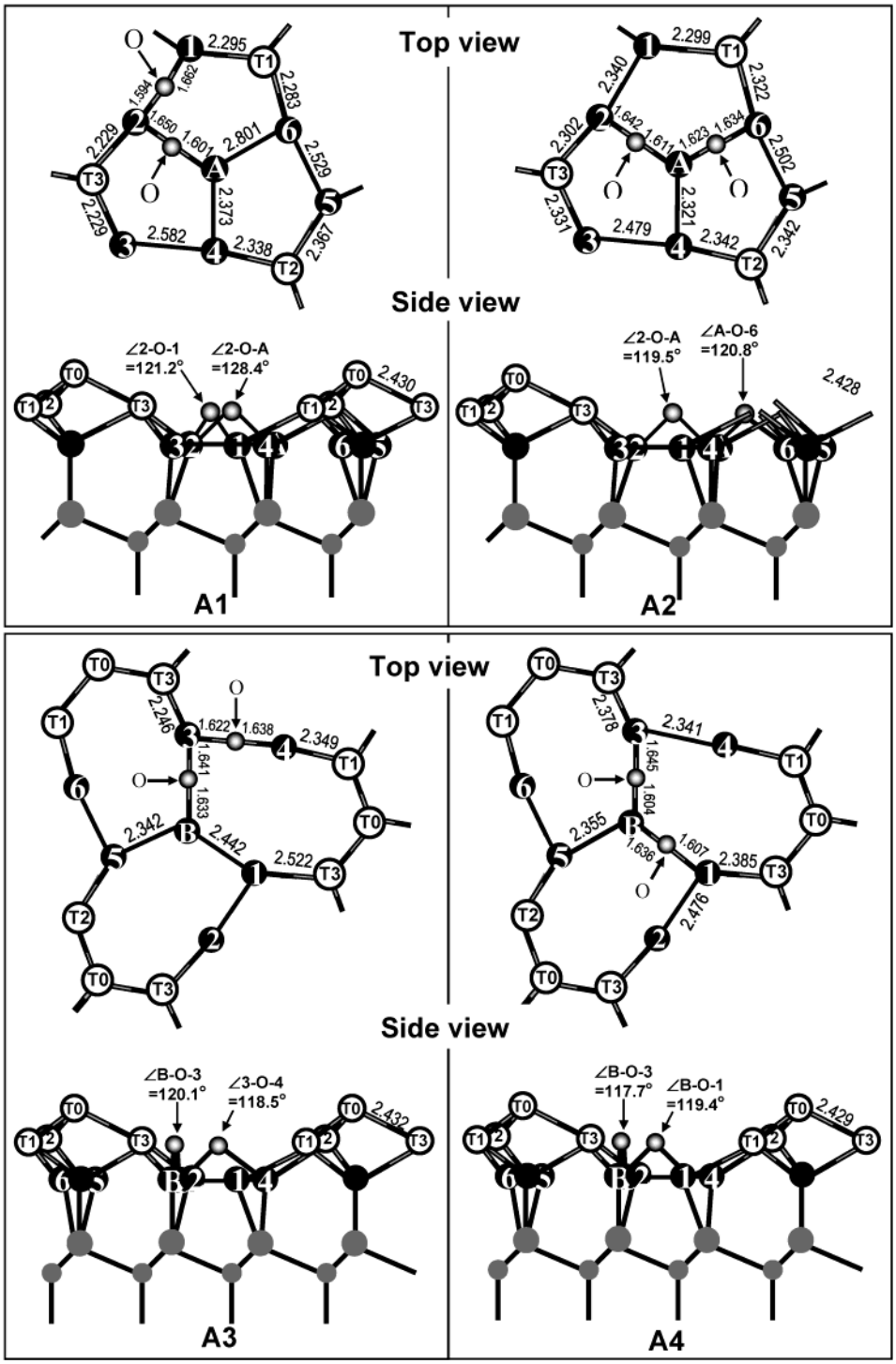

Figure 8. Possible configurations for the chemisorption of one O_2 per 3 × 3 unit cell at the adlayer sites on the SiC(0001)-3×3 surface.

3.3. Calculated DOS of O/SiC 3 × 3 Surface. 3.3.1. LDOS of the SiC 3 × 3 Surface. Figure 9a shows the calculated total density of states (TDOS) of the clean SiC 3 × 3 surface where the zero binding energy scale is referenced to the valence band maximum (VBM). The layered projected DOS (LDOS) in Figure 9b(i) shows a sharp filled state peak at the VBM originating from the dangling bond which is located on the first-layer T0 atom. This state has hybridized sp^3 characteristics as judged from the strong p and weak s character, in accordance with the proposed tetrahedral bonding. Tunneling from VBM dangling bond states has been suggested to be responsible for the bright spot in the filled state STM image, where every 3 × 3 unit cell is characterized by a bright spot. The LDOS of the second layer T1 shows small density at the VBM due to charge transfer from T0. Interestingly, the LDOS of the third layer shows different DOS for atom A and atom 4 which reflects their different bonding geometry. The enhanced p-state near VBM for atom A in Figure 9b(iii) arises from its coplanar bond nature, as shown in Figure 8. For the fourth layer bulk Si atom which adopts typical tetrahedral bonding, the p-state below the VBM is rather weak as shown in Figure 9b(v). It can be inferred that the coplanar bonds at site A and B involve mainly the p−p overlap with the bond axis parallel to surface plane.

3.3.2. LDOS of Oxygenated SiC. Adsorption of oxygen (two oxygen atoms) initially, to form the C1, C2, or C3 models, saturates the silicon dangling bond and results in the decrease

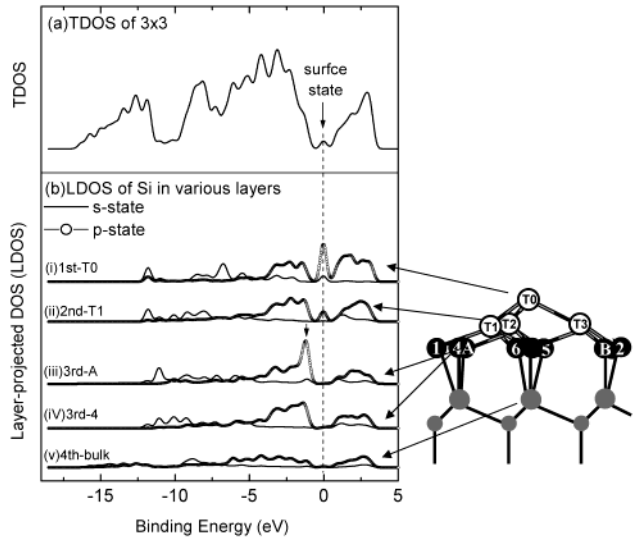

Figure 9. (a) Total DOS (TDOS) of SiC-3× 3 surface. (b) Layer-projected DOS (LDOS) of (i) T0 atom in the first layer, (ii) T1 atom in the second layer, (iii) atom "A" in the third layer, (iv) atom "4" in the third layer, and (v) Si atom in the fourth bulk layer.

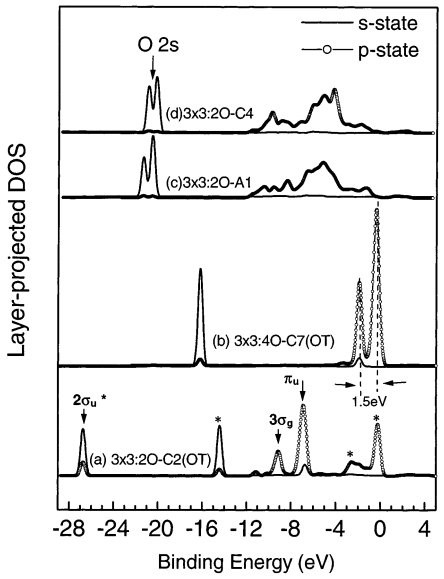

Figure 10. Layer-projected DOS calculated for oxygen adopting various configurations: (a) 3×3:2O−C2 surface (on-top oxygen); (b) 3×3:4O−C7 surface (on-top oxygen); (c) 3×3:2O−A1 surface (bridge oxygen); (d) 3×3:2O−C4 surface (bridge oxygen).

of electron density at the VBM. First we look at the LDOS of oxygen adopting different chemisorption state. If the oxygen adsorbs in a molecular precursor state, as in model C2, sharp molecular states that correspond to free O_2 state can be seen. Figure 10a shows that the on-top O−O peroxy species produces strong DOS at −26.7, +9.4, and −6.9 eV which are attributable to the O_2 molecular orbitals. All models where the oxygen adopts an *on-top* configuration give rise to sharp state at the VBM due to O 2p orbitals. This applies also to the LDOS of model C7 where a tetrahedral SiO_4 type cluster (refer to Figure 7) is formed, as shown in Figure 10b. For these "on-top" configurations, however, the corresponding LDOS of the T0 Si atom will show a decrease in DOS intensity at VBM since the O atom saturates the dangling bond. For models where oxygen inserts into the back-bonds to form Si−O−Si type bonding (eg. C4 model), parts c and d of Figure 10 show that

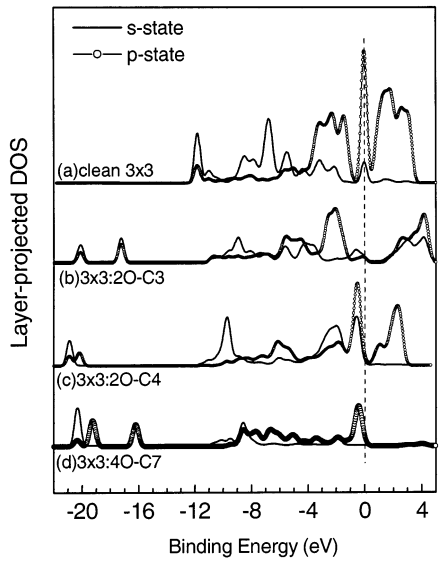

Figure 11. LDOS of topmost Si T0 atom calculated for (a) clean 3 × 3, (b) 3×3:2O−C3 model, (c) 3×3:2O−C4 model, and (d) 3×3:4O−C7 model surfaces

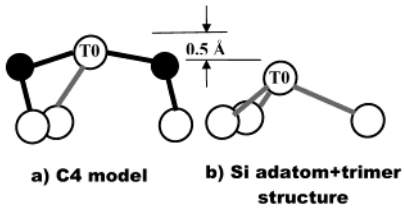

Figure 12. C4 models (a) for O_2 adsorption on the Si adatom−trimer structure (b) of the 6H−SiC(0001)-3×3 surface. The white and dark circles represent Si and O atoms, respectively.

the O LDOS is characterized by a weaker emission state at the VBM and the appearance of an O 2*s* state at 21 eV.

Tunneling from VBM dangling bond states has been suggested to be responsible for the bright spot in the filled state STM image, where every 3 × 3 unit cell is characterized by a bright spot.[7,8] The tunneling current contrast variations in an STM image depend on the density of states (DOS) at a particular site *I*, as well as energy *E*, and the height above the surface z.[21] An oxidation reaction at site *i* can change not only the DOS but also *z* if oxygen atoms were inserted into the Si−Si bonds. Figure 11 shows the LDOS of the topmost Si T0 atom, where part a corresponds to the clean 3 × 3, showing the strong dangling bond state at the VBM. This may explain why the electrophilic attack by oxygen selectively occurs on these adatom sites. The adsorption of oxygen in the manner that gives rise to C1, C2, or C3 models passivates the dangling bond state (DOS) as shown in Figure 11b and induces the formation of the dark sites at the initial oxidation stage. Our total energy calculations reveal that at the coverage of two oxygen atoms per unit cell, structure C4 which arises from the insertion of two oxygen atoms in the Si back-bonds to form two Si−O−Si structures, is the *most stable structure* among all configurations considered. According to the calculated structural data, the T0 Si adatom in the C4 model protrudes into the vacuum region by 0.50 Å ($\delta z = 0.50$ Å) compared to the unreacted adatoms, as shown in Figure 12. Therefore, these adatoms may appear brighter than the unreacted sites in STM image. With an increase in the oxygen coverage on the surface, we observed an initial increase in the density of dark sites in the STM images, and this is subsequently followed by the appearance of bright sites. For models with higher oxygen incorporation, the LDOS shows

an increase in the filled state density near the VBM in Figure 11, parts c and d. For example, in the tetrahedral SiO_4 structure (structure C7), a peak near the VBM can be seen in Figure 11d for the LDOS of the top T0 atom. The increase in the electron density of the T0 Si atom is attributable to charge transfer from the oxygen, as judged from the purely p-type state near VBM. The peak at VBM is mirrored by the −0.4 and −1.9 eV peaks of the O LDOS, attributable to the $2p_x$ and $2p_y$ orbitals.[22] The increase in DOS near the VBM may be correlated to the appearance of bright spots in the STM after the increase in oxygen dosage.

Therefore the change in the DOS near the VBM with different oxygen configurations suggests a dip in the intensity of the tunneling current from VBM at first due to the removal of the dangling bond state. The subsequent insertion of oxygen into the Si back-bonds of the adatom clusters will recover the filled state density near the VBM, and contributes to the appearance of "bright" sites in the STM images. This agrees well with our observation of the appearance of *dark sites* initially in the STM images, and the subsequent increase in the density of *bright sites* in the STM images with an increase in surface oxygen coverage.

Our DFT calculations are inconsistent with the interpretations of Amy et al.[12] who suggested that molecular oxygen preferentially attacks the third adlayer at atom A during the initial oxidation stage. We can see two major arguments for oxygen adsorption at the adatom site instead of the adlayer site. Preferential adsorption of oxygen at the adatom cluster site over adlayer site can be explained by the less sterically hindered geometry of the former compared to the latter. The presence of the dangling bond on the adatom also favors the dissociation of O_2. In fact, an isolated O_2 molecule needs an energy of 118.3 kcal/mol to dissociate into atomic oxygen,[23] while the activation energy for O_2 adsorption on the Si(111)-7×7 dangling bond site was calculated to be only half this value.[24] Hattori et al.[25] verified that only one of the 10^9 incident O_2 molecules could contribute to the oxidation of Si(111):H surface when the Si dangling bonds were saturated by H atoms. O_2 chemisorption will be energetically more prohibitive on the adlayer site due to the lower O_2 sticking probability and higher reaction activation energy at these sites. We therefore propose that the changes in the STM images during the initial oxidation stage must be related to changes in DOS of the silicon adatoms with oxygen adsorption.

4. Conclusion

We have investigated the initial stage oxygenation reactions of the 6H−SiC(0001)3×3 surface with oxygen molecules. Our combined STM and periodic-DFT calculations suggest that O_2 molecules selectively adsorb at the adatom cluster site on the 6H−SiC(0001)3×3 surface, and subsequently undergo dissociation and insertion into the Si−Si back-bond to form the Si−O−Si bridge configuration in SiO_4. This indicates that the initial reaction pattern is similar to the oxygenation reaction on the Si(111)-7×7 surface where changes in the adatom dangling bond state observed in valence band photoemission as well as STM studies support the proposal that reaction proceeds initially at the reactive adatom cluster site.[26,27] Atomic O beam treatment of the surface and subsequent annealing resulted in the formation of silicon oxide nanoclusters on the surface.

References and Notes

(1) Sheppard, M. Melloch,; Cooper, J., Jr. *IEEE Trans. Electron Devices* **1994**, *41*, 1257.
(2) Ueno, K.; Asai, R.; Tsuji, T. *IEEE Trans. Electron Device Lett.* **1998**, *19*, 244.
(3) Lipkin, L.; Slater, D., Jr.; Palmour, J. *Mater. Sci. Forum.* **1998**, 264−268, 853.
(4) Afanas'ev, V.; Bassler, M.; Pensl, G.; Schulz, M. *Phys. Stat. Solidi* **1997**, A *162*, 321.
(5) Kaplan, R. *Surf. Sci.* **1989**, *215*, 111.
(6) Kulakov, M. A.; Henn, G.; Bullemer, B. *Surf. Sci.* **1996**, *346*, 49.
(7) Starke, U.; Schardt, J.; Bernhardt, J.; Franke, M.; Reuter, K.; Wedler, H.; Heinz, K. *Phys. Rev. Lett.* **1998**, *80*, 758.
(8) Schardt, J.; Bernhardt, J.; Starke, U.; Heinz, K. *Phys. Rev. B.* **2000**, *62*, 10335.
(9) Tanaka, S.; Kern, R. S.; Davis, R. F. *Appl. Phys. Lett.* **1994**, *65*, 2851.
(10) Fissel, A.; Schröter, B.; Richter, W. *Appl. Phys. Lett.* **1995**, *66*, 3182.
(11) Furthmüler, J.;Bechstedt, F. *Phys. Rev. B* **1998**, *58*, 13712.
(12) Amy, F.; Enriquez, H.; Soukiassian, P.; Storinio, P.-F.; Chabal, Y. J.; Mayne, A. J.; Dujardin, G.; Hwu, Y. K.; Brylinski, C. *Phys. Rev. Lett.* **2001**, *86*, 4342.
(13) Ong, W. J.; Tok, E. S.; Xu, H.; Wee, A. T. S. *Appl. Phys. Lett.* **2002**, *80*, 3406.
(14) Xie, X. N.; Wang, H. Q.; Wee, A. T. S.; Loh, K. P. *Surf. Sci.* **2001**, *478*, 57.
(15) Loh, K. P.; Xie, X. N.; Lim, Y. H.; Teo, E. J.; Zheng, J. C.; Ando, T. *Surf. Sci.* **2002**, *505*, 93.
(16) Peter, M.; Payne, M.; Allan, D. *Phys. Rev. B.* **1989**, *40*, 12255.
(17) Polak, E. *Computational Methods in Optimization*; Academic: New York, 1971; p 56.
(18) Burke, K.; Perdew, J.; Levy, M. *Modern Density Functional Theory: A Tool for Chemistry*, Seminario, J., Politzer P., Eds.; Theoretical and Computational Chemistry 2; Elsevier: New York, 1995; pp 29−74.
(19) Amy, F.; Soukiassian, P.; Hwu, Y. K.; Brylinski, C. *Appl. Phys. Lett.* **1999**, *75*, 3360.
(20) Amy, F.; Soukiassian, P.; Hwu, Y. K.; Brylinski, C. *Surf. Sci.* **2000**, *464*, L691.
(21) Wiesendanger, R.; Guntherodt, H.-J.; et al. *Scanning tunneling microscopy III: theory of STM and related scanning probe methods*; Springer: Berlin and New York, c1996.
(22) Lee, S.-H.; Kang, M.-H. *Phys. Rev. Lett.* **1999**, *82*, 968.
(23) CODATA recommended key values for thermodynamics. *J. Chem. Thermodyn.* **1978**, *10*, 903.
(24) Hoshino, T. *Phys. Rev. B.* **1999**, *59*, 2332.
(25) Hattori, T.; Butsuri, O. **1995**, *64*, 1085.
(26) Bozso, F.; Avouris, Ph. *Phys. Rev. B.* **1991**, *44*, 9129.
(27) Pelz, J. P.; Koch, R. H. *Phys. Rev. B.* **1990**, *42*, 3761.
(28) Kubo, O.; Kobayashi, T.; Yamaoka, N.; Itou, S.; Nishida, A.; Katayama, M.; Oura, K. *Surf. Sci.* **2003**, *529*, 107.